Assessing the defect responsible for LeTID: temperature- and injection-dependent lifetime spectroscopy

Mallory A. Jensen[1], Yan Zhu[2], Erin E. Looney[1], Ashley E. Morishige[1], Carlos Vargas[2], Ziv Hameiri[2], Tonio Buonassisi[1]

[1]Massachusetts Institute of Technology, Cambridge, MA 02139, USA, email: jensenma@alum.mit.edu
[2]University of New South Wales, Sydney, NSW 2052, Australia

***Abstract* — Temperature- and injection-dependent lifetime spectroscopy (TIDLS) is employed to study the defect responsible for light- and elevated temperature-induced degradation (LeTID). In our previous analyses, titanium (Ti), molybdenum (Mo), and tungsten (W) were identified as potential candidates for LeTID. The addition of temperature dependence further constrains the defect parameters. Assuming constant defect parameters with temperature, we identify two possible sets of defect parameters: k = 23.9 ± 5.5 at E_t-E_i = -0.21 ± 0.06 eV and k = 23.5 ± 5.6 at E_t-E_i = -0.10 ± 0.07 eV. We consider our results in the context of published defect parameters identified by TIDLS in other LeTID samples, and we evaluate our results against reported defect parameter temperature dependencies for Ti and Mo. We conclude that Mo is most consistent with our measurements. Approaches beyond lifetime spectroscopy, including intentional contamination and chemical composition measurements, are required to determine the root cause of LeTID.**

***Index Terms* — bulk lifetime, carrier-induced degradation, lifetime spectroscopy, light- and elevated temperature-induced degradation (LeTID), light-induced degradation, materials reliability, multicrystalline silicon (mc-Si).**

I. PERC LeTID: Identifying Root Cause

Light- and elevated temperature-induced degradation (LeTID) can cause approximately 10% relative efficiency degradation in multicrystalline silicon (mc-Si) PERC solar cells within the first months of operation [1]. While mitigation strategies for LeTID (*e.g.* accelerated degradation and regeneration [2]–[4]) have been suggested and proven, the root cause of LeTID is still unknown. Uncertainty about the root cause of LeTID necessitates process- and/or material-specific optimization of the proposed engineering solutions, which can be costly and time-consuming. Pinpointing the root cause of LeTID is critical to developing targeted solutions that maximize device efficiency.

The LeTID defect has been hypothesized to be a ubiquitously-distributed bulk defect [5]–[7]. Lifetime spectroscopy analysis of room-temperature injection-dependent lifetime curves for samples in the degraded state suggests three potential candidates known to be present during the silicon feedstock refining and growth processes: titanium (Ti), molybdenum (Mo), and tungsten (W). The identification of these candidates is dependent on comparison of calculated defect parameters with those reported by deep-level transient spectroscopy (DLTS) or otherwise in the literature. A further investigation of the defect parameters is warranted due to experimental evidence of getterability of the LeTID defect [8], which is not necessarily compatible with such slow diffusers as W [9].

In this contribution, we extend our previous lifetime spectroscopy analyses to consider quantitatively the temperature- and injection-dependent lifetime of the LeTID defect. We identify one possible set of defect parameters in each bandgap half: k = 23.9 ± 5.5 at E_t-E_i = -0.21 ± 0.06 eV (more likely) and k = 23.5 ± 5.6 at E_t-E_i = 0.10 ± 0.07 eV (less likely). However, we note that the defect parameters are probably temperature-dependent, which impedes identification of the energy levels. Based on comparisons to reported temperature dependencies of the defect parameters for Mo and Ti (W has not yet been studied), we find that Mo is consistent with our measurements. We propose further experiments, beyond lifetime spectroscopy, to discern whether Mo is responsible for LeTID and whether there are any additional candidate defects.

II. TIDLS Measurement and Analysis Methods

The samples used in this study are taken from the same wafers as those described in Refs. [5]–[7]. Two adjacent *p*-type mc-Si wafers, grown by directional solidification with resistivity 1.6 Ω-cm and thickness 175 μm, were selected. These wafers were prepared as PERC semifabricates, with front side silicon nitride (SiN_x) passivated emitter and rear side oxide/SiN_x stack. Both wafers were fired at 950°C (actual sample temperature ≈850°C). To isolate the defect responsible for LeTID, one wafer was stored in the dark (undegraded) and one wafer was subjected to degradation conditions (65-75°C and 0.9-1.1 suns) for 168 hours (degraded).

Temperature- and injection-dependent lifetime spectroscopy (TIDLS) measurements were completed at the University of New South Wales with a lifetime tester equipped with a temperature-controlled cryostat, photoconductance coil, and a standard Xenon flash lamp for illumination [10], [11]. Measurements were acquired at sample setpoint temperatures 25°C, 50°C, 100°C, 150°C, and 200°C. Since the LeTID defect is known to be metastable at 200°C, room-temperature QSSPC measurements were completed after each elevated temperature measurement with a Sinton Instruments WCT-120.

Lifetime spectroscopy analysis is carried out as described in Refs. [6], [12], [13]. We assume that the LeTID defect is

978-1-5090-5605-7/17/$31.00 ©2017 IEEE

responsible for the lifetime difference between the undegraded and degraded wafers and that recombination at the defect can be described by Shockley-Read-Hall (SRH) statistics. For each temperature, the injection-dependent SRH lifetime is determined according to the inverse harmonic difference between the two lifetimes:

$$\tau_{SRH} = \left(\frac{1}{\tau_{deg}} - \frac{1}{\tau_{undeg}}\right)^{-1}$$

An important assumption underlying this approach is that background recombination mechanisms, including surface, radiative, Auger, and other SRH defects, are identical at each temperature between the two samples. The SRH lifetime is then linearized [13], and a two-defect fit that minimizes the χ^2 error between the measured and fit SRH lifetimes is used to identify possible defect parameters. The electron-to-hole capture cross-section ratio ($k = \sigma_n/\sigma_p$) and electron capture time-constant (τ_{n0}), which is a function of electron capture cross-section (σ_n), defect concentration (N_t), and thermal velocity (v_{th}), are calculated as functions of possible defect levels within the bandgap. The defect level is referenced to the intrinsic level, as in Ref. [11].

III. Lifetime Measurements

A. TIDLS measurements

Injection-dependent lifetime measurements at each elevated temperature are shown in Figs. 1(a) and (c) for both samples. As previously reported in Ref. [6], the injection dependence (*i.e.* the shape of the curve) of the LeTID defect, represented by the degraded sample [Fig. 1(a)], does not change significantly as the sample temperature increases. The lifetime changes significantly in magnitude at 200°C. A corresponding change in lifetime can be observed in the undegraded sample [Fig. 1(c)].

B. Measurements after TIDLS

To assess the stability of the LeTID defect, room-temperature QSSPC measurements were completed after each elevated temperature measurement [Figs. 1(b) and (d)]. The room-temperature lifetimes increase and decrease after the 200°C measurement for the degraded and undegraded samples, respectively. The lifetime change for the undegraded sample begins as low as 150°C. Similar results have been observed after dark annealing of undegraded samples at temperatures up to 250°C [14].

One possible explanation for the change in room temperature lifetime [Figs. 1(b) and (d)] is that the undegraded sample experiences an accelerated degradation while at high temperature and under illumination from the flash lamp. Similarly, the degraded sample may experience an accelerated regeneration. However, since a dark anneal performed in the degraded state is known to reverse the LeTID defect to its initial condition [5], [15], [16], the lifetime measured after 200°C for the degraded sample may correspond instead to an intermediate state. Vargas, Zhu *et al.* avoided the issue of metastable defect configurations by measuring below room temperature up to 75°C [11].

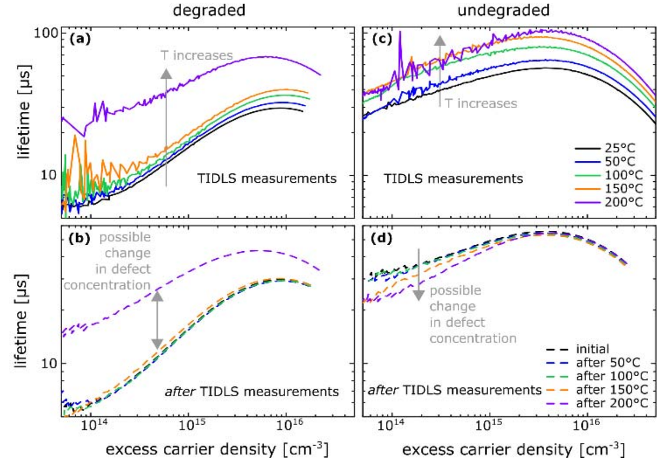

Fig. 1: (a) and (c): Injection-dependent lifetime measurements at setpoint temperatures 25°C, 50°C, 100°C, 150°C, and 200°C for the degraded and undegraded samples, respectively. (b) and (d): Room-temperature injection-dependent lifetime measurements performed after each elevated temperature measurement to demonstrate the stability of the LeTID defect.

In either case, similar injection dependence can still be observed in the degraded sample after the 200°C measurement. Lifetime spectroscopy analysis of the measurements after each TIDLS temperature indicates that a defect with nearly identical E_t-E_i vs. k dominates the room temperature degraded lifetimes. The k-values at midgap for the dominant defect are 27.9, 29.7, 30.7, and 30.1 for the degraded measurements after 50°C, 100°C, 150°C, and 200°C, respectively. If the defect is still present in the sample after each elevated temperature measurement (same E_t-E_i, k), the possible change in state after this measurement would influence calculation of τ_{n0} ($1/\sigma_n N_t v_{th}$) rather than k. A changing LeTID defect concentration would then account for the lifetime difference between samples as temperature is increased, similar to the trend observed during degradation and regeneration in Ref. [7]. The change in lifetime of the undegraded sample [Fig. 1(d)] is too small for reliable analysis; however, these curves are also expected to be dominated by a similar defect (but lower concentration) if degradation starts during the measurement, as in Ref. [7]. Therefore, we do not exclude the 200°C measurement from further discussion.

IV. Calculated Defect Parameters

The results of the defect fitting procedure for the SRH lifetime are shown in Fig. 2. Defects with comparable k-values are plotted in red (see Refs. [9], [17]–[19]). If the k-value is not temperature-dependent, the true defect parameters can be determined from the intersection of the E_t-E_i vs. k curves [12]. At every temperature, there is one defect that dominates the

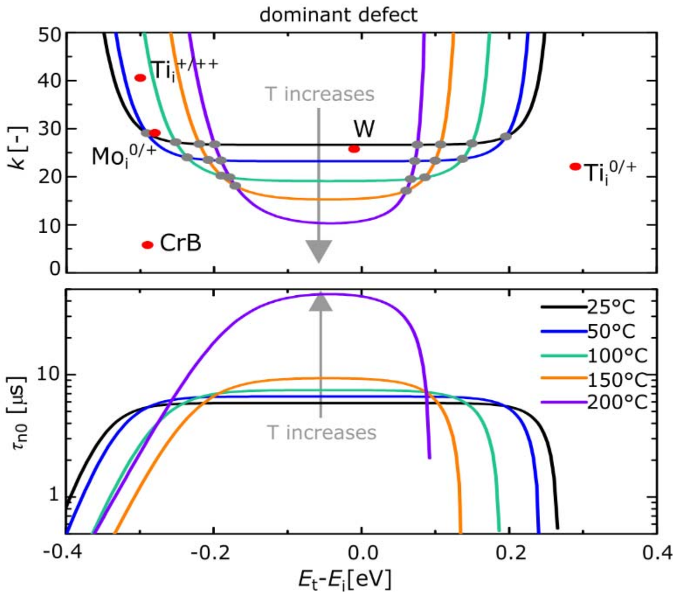

Fig. 2: Calculated LeTID defect parameters at each measured temperature, with no clear intersection point for all curves. (top): k-value (electron-to-hole capture cross-section ratio) as a function of energy level. Intersection points between curves are marked with gray circles. Reported defect parameters are plotted in red for comparison. (bottom): τ_{n0} (electron capture time constant) as a function of energy level.

lifetime signature throughout the measured injection range and would therefore be dominant under solar cell operating conditions. This defect is most likely to be the LeTID defect; therefore, we focus the discussion on the dominant defect. Defect 2 (not shown) is a shallow defect with no clear intersection points between E_t-E_i vs. k curves measured at different temperatures.

All possible curve intersections are plotted as gray circles on Fig. 2(top). There are several quantitative ways to evaluate possible intersections and thus defect parameters from TIDLS measurements [12], [20]. For example, the mostly likely intersection points may correspond to the minimum standard deviation of the k-values at each energy level. Using this approach, two local minima can be identified: k = 22.8 ± 3.2 at -0.19 eV (lower bandgap half) and k = 21.9 ± 4.4 at 0.07 eV (upper bandgap half). The error in the k-value is assigned based on the range of k-values at the local minimum. If the 200°C measurement is excluded, the two local minima are k = 24.2 ± 2.7 at -0.21 eV and k = 23.7 ± 3.1 at 0.10 eV. In both cases, the intersection in the lower bandgap half has a lower standard deviation, which may indicate that the true defect level resides in the lower bandgap half.

However, as shown in Fig. 2, there is not a single distinct intersection for all curves. Considering all possible intersections points, the average intersection points are at k = 23.9 ± 5.5 at -0.21 ± 0.06 eV and k = 23.5 ± 5.6 at 0.10 ± 0.07 eV. Here, the error in both k-value and energy level are defined by the ranges for all intersection points in each bandgap half.

We note that the energy levels and k-values reported herein are inconsistent with those identified by Vargas, Zhu, *et al*. (k = 56 ± 23 at -0.32 ± 0.05 eV and k = 49 ± 21 at 0.21 ± 0.05 eV) [11]. This inconsistency is likely due to uncertainties in the measuring and fitting procedures. For example, there may be changes in background recombination mechanisms (*e.g.* surface recombination) and/or differences in material quality (*e.g.* dislocation density and related recombination), both of which are not explicitly accounted for in the analysis presented herein. It is also possible that the defect, although similar in nature, is not exactly the same between the two sample sets, or that the net recombination of the defect, although similar at room temperature, varies at elevated temperatures due to the changing defect concentration (see Section III). The similarities and differences between the two sample sets will be discussed further in the next section.

Fig. 2(bottom) shows the electron capture time-constant as a function of energy level. As discussed in the previous section, the electron capture time-constant increases significantly at 200°C. This is likely related to a decrease in LeTID defect concentration, ra E_t-E_i vs. k ther than a change in the dominant defect itself.

V. Comparison to Literature Values: Titanium & Molbydenum

Since the defect does not demonstrate a clear intersection point for all curves, there are three possibilities: (1) uncertainty in the measuring and fitting procedures masks the intersection point, (2) the defect itself changes during the measurement, or (3) one or both of the capture cross-sections may be temperature-dependent. The first possibility was quantified and discussed in the previous section.

The second possibility is not a likely explanation for the lack of a clear intersection. In previous work, we reported that changes in recombination during most of degradation and regeneration are due to a change in concentration of a single defect [7]. Although we observe a change in the room-temperature lifetime after the TIDLS measurements, it is likely that the underlying defect is still the same, with the same k-value but different concentration. We therefore assess the second possibility here.

To assess the third possibility, we compare the temperature dependencies of the k-values reported in literature for two possible LeTID defect candidates, Ti and Mo [5], [6], to our calculated values at the defect-relevant energy level (reference defect parameters: Ti [17] and Mo [21]). It should be noted that the reference Ti k-value was only measured at high temperatures (140–270°C) [17], while the reference Mo k-value was measured over a wider range (-110–150°C) [21]. For the purposes of comparison with experimental data, the reference trend for Ti is extrapolated to temperatures down to -25°C. The other proposed defect candidate, W, is excluded from this analysis because an equivalent study has not yet been conducted. We include the measurements reported in Ref. [11], processed with the same algorithms used herein, in this

comparison to further assess any inconsistency between our results.

Figs. 3 and 4 show the results for the k-value as a function of temperature for Ti and Mo, respectively. When evaluated at the defect-relevant energy level, the k-values reported by the two studies (this abstract and Vargas, Zhu *et al.* [11]) are consistent. The measured trend is inconsistent with that predicted for Ti (Fig. 3), as the measured k-value remains constant and increases as temperature drops from 75°C to below room temperature. While the measured k-values are not an exact match for Mo (Fig. 4), the measured trend with temperature is consistent with reported values.

An additional metric for evaluating these candidates is the temperature dependence of the electron capture cross-section (σ_n), which can be derived from τ_{n0}. Representative defect concentrations can be calculated at room temperature, using the thermal velocity [12] and the literature values for σ_n. For the data reported herein, these concentrations are 6.4 and 1.2×10^{12} cm^{-3} for Ti and Mo, respectively. For the data reported in Ref. [11], the same concentrations are 2.6×10^{12} and 4.8×10^{11} cm^{-3}. Assuming a constant defect concentration up to 150°C, σ_n is calculated as a function of temperature for both defects [Figs. 3 and 4 (bottom)]. Values above 150°C are not included due to the possible change in defect concentration. Reported temperature dependencies for each capture cross-section are also plotted (Ti [17] and Mo [21]).

Both experimental data sets shown in the bottom plots of Figs. 3 and 4 match the reference values at room temperature due to the method of calculation. The experimental results are most consistent with the reported trend and values (away from room temperature) for Mo. Unlike the k-value, the reference temperature-dependence of the capture cross-section for Ti is derived from a model, valid in a wider temperature range [17].

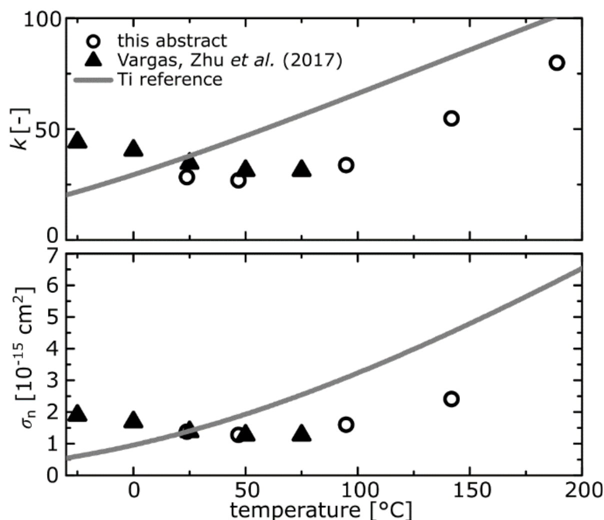

Fig. 3: (top) k-value calculated from the results shown in Fig. 2 as a function of temperature at the Ti energy level. Experimental data from this abstract is compared to published data from similar samples [11] and reported literature values [17]. (bottom) Electron capture cross-section calculated from Fig. 2 as a function of temperature at the Ti energy level, assuming a constant defect concentration that is calculated at room-temperature.

The reference trend at lower temperatures is therefore expected to be more accurate for σ_n than for the k-value. For these reasons, we conclude that Mo is a more likely candidate for the LeTID defect than Ti.

If Mo is responsible for LeTID, it is unlikely that the gettering response observed by Zuschlag *et al.* is due to gettering of the LeTID defect [8]. The pronounced difference in degradation and regeneration between as-grown and gettered samples could instead be due to process differences (*e.g.* firing with an emitter for the gettered samples), perhaps modifying the LeTID defect and/or surface passivation quality. Rohatgi *et al.* observed no difference in the detrimental effect of Mo on solar cell performance after annealing at 1100°C [22]. Additionally, compared to iron, which is known to be getterable, Mo has a very low diffusivity [9], [23]. Therefore, we do not expect changes in the Mo distribution or total concentration to explain the observed gettering response.

It is possible that the true LeTID defect has similar parameters and temperature dependencies to Mo and has not yet been studied by DLTS or lifetime spectroscopy. While this study fully utilizes the potential of TIDLS, to progress further in identifying the root cause of the LeTID, a new approach is required. Targeted experiments, either through intentional contamination or through chemical composition measurements of LeTID-affected samples, should be conducted to assess current candidates and identify additional candidates.

VI. Summary

In this contribution, we present quantitative analysis of the temperature- and injection-dependent lifetime of p-type mc-Si affected by LeTID. By using adjacent degraded and undegraded wafers from the same ingot, we isolate the SRH lifetime

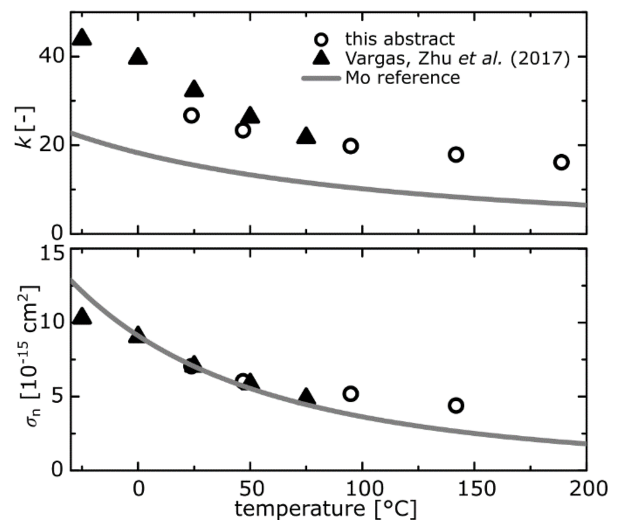

Fig. 4: (top) k-value calculated from the results shown in Fig. 2 as a function of temperature at the Mo energy level. Experimental data from this abstract is compared to published data from similar samples [11] and reported literature values [21]. (bottom) Electron capture cross-section calculated from Fig. 2 as a function of temperature at the Mo energy level, assuming a constant defect concentration that is calculated at room-temperature.

associated with the LeTID defect and analyze this lifetime for possible defect parameters. We find that one defect is dominant throughout the measured injection range at each temperature, and this defect has parameters consistent with those previously reported for the LeTID defect at room temperature. Quantitative analysis suggests that one or both of the capture cross-sections are temperature-dependent, and that the observed temperature dependencies are more consistent with reported values for Mo than for Ti, two defects previously identified as LeTID defect candidates. We suggest that the defect responsible for LeTID has not yet been studied by DLTS or other electrical characterization techniques, and we propose further investigation *via* intentional contamination and/or chemical composition measurements to assess candidates.

ACKNOWLEDGEMENT

This material is based upon work supported in part by the National Science Foundation (NSF) and in part by the Department of Energy under NSF CA No. EEC-1041895. This work was also supported by the Australian Government through the Australian Renewable Energy Agency (ARENA, Project 2014/RND097). The work of M. A. Jensen and E. E. Looney was supported by the NSF Graduate Research Fellowship under Grant 1122374. The work of M. A. Jensen was further supported by the NSF Graduate Research Opportunities Worldwide Fellowship for travel to the University of New South Wales. Z. Hameiri acknowledges the support of the Australian Research Council (ARC) through the Discovery Early Career Researcher Award (DECRA, Project DE150100268).

REFERENCES

[1] F. Kersten *et al.*, "Degradation of multicrystalline silicon solar cells and modules after illumination at elevated temperature," *Sol. Energy Mater. Sol. Cells*, vol. 142, pp. 83–86, 2015.

[2] C. E. Chan *et al.*, "Rapid Stabilization of High-Performance Multicrystalline p-type Silicon PERC Cells," *IEEE J. Photovoltaics*, vol. 6, no. 6, pp. 1473–1479, 2016.

[3] D. N. R. Payne *et al.*, "Rapid passivation of carrier-induced defects in p-type multi-crystalline silicon," *Sol. Energy Mater. Sol. Cells*, vol. 158, pp. 102–106, 2016.

[4] D. N. R. Payne *et al.*, "Acceleration and mitigation of carrier-induced degradation in p-type multi-crystalline silicon," *Phys. Status Solidi - Rapid Res. Lett.*, vol. 10, no. 3, pp. 237–241, 2016.

[5] K. Nakayashiki *et al.*, "Engineering Solutions and Root-Cause Analysis for Light-Induced Degradation in p-type Multicrystalline Silicon PERC Modules," *IEEE J. Photovoltaics*, vol. 6, no. 4, pp. 860–868, 2016.

[6] A. E. Morishige *et al.*, "Lifetime Spectroscopy Investigation of Light-Induced Degradation in p-type Multicrystalline Silicon PERC," *IEEE J. Photovoltaics*, vol. 6, no. 6, pp. 1466–1472, 2016.

[7] M. A. Jensen *et al.*, "Evolution of LeTID Defects in p-type Multicrystalline Silicon During Degradation and Regeneration," *IEEE J. Photovoltaics*, vol. PP, no. 99, pp. 1–8, 2017.

[8] A. Zuschlag, D. Skorka, and G. Hahn, "Degradation and regeneration in mc-Si after different gettering steps," *Prog. Photovolt Res. Appl.*, pp. 1–8, 2016.

[9] K. Graff, Metal Impurities in Silicon-Device Fabrication, 2nd ed. New York, New York: Springer-Verlag, 2000.

[10] Y. Zhu, M. A. Jensen, C. Vargas, G. Coletti, and Z. Hameiri, "Defect characterization via temperature and injection dependent lifetime spectroscopy," in Presentation at *9th International Workshop on Crystalline Silicon for Solar Cells*, 2016.

[11] C. Vargas, Y. Zhu *et al.*, "Recombination parameters of lifetime-limiting carrier-induced defects in multicrystalline silicon for solar cells," *Appl. Phys. Lett.*, vol. 110, no. 9, p. 92106, 2017.

[12] S. Rein, Lifetime Spectroscopy: A Method of Defect Characterization in Silicon for Photovoltaic Applications. Springer, 2005.

[13] J. D. Murphy *et al.*, "Parameterisation of injection-dependent lifetime measurements in semiconductors in terms of Shockley-Read-Hall statistics : An application to oxide precipitates in silicon," *J. Appl. Phys.*, vol. 111, no. 113709, 2012.

[14] C. Chan *et al.*, "Modulation of Carrier-Induced Defect Kinetics in Multi-Crystalline Silicon PERC Cells Through Dark Annealing," *Sol. RRL*, p. 1600028, 2017.

[15] K. Krauss, A. A. Brand, F. Fertig, S. Rein, J. Nekarda, and E. Sytems, "Fast regeneration processes to avoid light-induced degradation in multicrystalline silicon solar cells," *IEEE J. Photovoltaics*, vol. 6, no. 6, pp. 1427–1431, 2016.

[16] F. Fertig, K. Krauss, and S. Rein, "Light-induced degradation of PECVD aluminium oxide passivated silicon solar cells," *Phys. Status Solidi - Rapid Res. Lett.*, vol. 9, no. 1, pp. 41–46, 2015.

[17] B. B. Paudyal, K. R. McIntosh, and D. H. MacDonald, "Temperature dependent carrier lifetime studies on Ti-doped multicrystalline silicon," *J. Appl. Phys.*, vol. 105, no. 12, 2009.

[18] C. Sun, F. E. Rougieux, and D. Macdonald, "Reassessment of the recombination parameters of chromium in n- and p-type crystalline silicon and chromium-boron pairs in p-type crystalline silicon," *J. Appl*, vol. 115, no. 21, p. 214907, 2014.

[19] S. Boughaba and D. Mathiot, "Deep level transient spectroscopy levels in silicon characterization of tungsten-related deep," *J. Appl. Phys.*, vol. 69, no. 1, pp. 278–283, 1991.

[20] Y. Zhu, Q. Thong, L. Gia, M. K. Juhl, G. Coletti, and Z. Hameiri, "Application of the Newton – Raphson Method to Lifetime Spectroscopy for Extraction of Defect Parameters," *IEEE J. Photovoltaics*, vol. PP, no. 99, pp. 1–6, 2017.

[21] B. B. Paudyal, K. R. McIntosh, D. H. MacDonald, and G. Coletti, "Temperature dependent carrier lifetime studies of Mo in crystalline silicon," *J. Appl. Phys.*, vol. 107, no. 5, pp. 2–6, 2010.

[22] A. Rohatgi, R. H. Hopkins, J. R. Davis, and R. B. Campbell, "The impact of molybdenum on silicon and silicon solar cell performance," *Solid. State. Electron.*, vol. 23, no. 11, pp. 1185–1190, 1980.

[23] J. L. Benton, "Behavior of Molybdenum in Silicon Evaluated for Integrated Circuit Processing," *J. Electrochem. Soc.*, vol. 146, no. 5, p. 1929, 1999.